PAPER

Tailoring Li$_6$PS$_5$Br ionic conductivity and understanding of its role in cathode mixtures for high performance all-solid-state Li–S batteries†

Chuang Yu,[ab] Jart Hageman,[a] Swapna Ganapathy,[a] Lambert van Eijck,[a] Long Zhang, [ID][c] Keegan R. Adair,[b] Xueliang Sun [ID] *[b] and Marnix Wagemaker [ID] *[a]

The ultrafast ionic conductivity of Li$_6$PS$_5$Br, which is higher than 1 mS cm^{-1} at room temperature, makes it an attractive candidate electrolyte for the all-solid-state Li–S battery. A simple synthesis route with an easy scale up process is critical for practical applications. In this work, the highest room temperature ionic conductivity (2.58 × 10^{-3} S cm^{-1}) of Li$_6$PS$_5$Br is obtained by an optimal annealing temperature in a simple solid-state reaction method. Neutron diffraction and XRD show that the origin of the highest ionic conductivity is due to the higher purity, smaller mean lithium ion jumps and the optimal Br ordering over 4a and 4c sites. All-solid-state Li–S batteries using a S–C composite cathode in combination with the optimized Li$_6$PS$_5$Br electrolyte and Li–In anode show high (dis)charge capacities. Different cycling modes (charge–discharge and discharge–charge) reveal that the capacity of the S–C–Li$_6$PS$_5$Br/Li$_6$PS$_5$Br/Li–In battery arises from both the active S–C composite and the Li$_6$PS$_5$Br in the cathode mixture. The contribution of the latter is verified from all-solid-state batteries using Li$_6$PS$_5$Br and its analogues as active materials. *Ex situ* XRD and electrochemical performance results show that the contribution of capacity from Li$_6$PS$_5$Br in the cathode mixture may be associated with the decomposition product Li$_2$S, while the Li$_6$PS$_5$Br in the bulk solid electrolyte layer is stable during cycling.

Introduction

Lithium ion batteries have been developed over the past few decades and are one of the most promising candidates for long-range hybrid electric vehicle (HEV) and electric vehicle (EV) applications.[1] Unfortunately, current lithium ion batteries utilize organic liquid electrolytes, which gives rise to safety issues associated with potential electrolyte leakage and the inherent flammability.[2] Unlike liquid organic electrolytes, solid electrolytes have high melting temperatures and contain inflammable components, leading to improved safety and durability. However, one of the obstacles for solid electrolytes is the low ionic conductivity compared to organic liquid electrolytes.

Numerous efforts have been devoted to finding solid Li-ion conductors with high ionic conductivities, a wide electrochemical stability window, and excellent chemical stability.[3] The Li-argyrodite Li$_6$PS$_5$X (X = Cl, Br and I) family is one of the

most promising electrolytes due to their high Li-ion conductivities in the range of 10^{-2}–10^{-3} S cm^{-1} at room temperature.[4–8] This conductivity is quite close to that of organic liquid electrolyte and the cost of the starting materials for Li-argyrodites are relatively cheap. The most commonly used synthesis route for this material is a high-energy milling process followed by heat-treatment.[9–13] Our previous work[8,10] showed that there are many challenges associated with this preparation method, such as time and energy consumption due to the high rotation speeds and long duration milling, which makes it difficult to scale up the production and limits its potential applications. Moreover, this mechanical milling method has a low repeatability and makes it difficult to obtain a homogenous solid electrolyte.[8] To address these challenges, the wet chemical synthesis route based on a dissolution-reprecipitation process was proposed.[14–19] Although this solution route provides a more homogeneous electrolyte with higher repeatability compared with the mechanical milling route, it still has other issues, such as the low ionic conductivity of the final sample[18,19] and/or the application of high-toxicity solvents during the preparation process.[16,17] Recently, we reported a simple solid-state method to obtain pure Li$_6$PS$_5$Cl having a high lithium ion conductivity without the use of the high rotation mechanical milling process.[7] For Li$_6$PS$_5$X (X = Cl, Br) synthesized from the mechanical milling followed by annealing route, the annealing temperature and the corresponding ionic conductivity for

[a]Department of Radiation Science and Technology, Delft University of Technology, Mekelweg 15, 2629JB Delft, The Netherlands. E-mail: m.wagemaker@tudelft.nl

[b]Department of Mechanical and Materials Engineering, University of Western Ontario, 1151 Richmond St, London, Ontario, N6A 3K7, Canada. E-mail: xsun9@uwo.ca

[c]State Key Laboratory of Metastable, Materials Science and Technology, Yanshan University, Qinhuangdao, Hebei 066004, China

Li_6PS_5Cl (550 °C) and Li_6PS_5Br (300 °C) are different.[8,10–13] Nevertheless, a number of questions remain unclear related to the electrolytes synthesized through solid-state sintering, including the relationship between annealing temperatures and ionic conductivity, structural evolution, and ionic dynamics.

Lithium sulfur batteries are a promising candidate for energy storage devices due to their high theoretical special capacity of 1675 mA h g^{-1}.[3,20] However, current lithium sulfur batteries using organic liquid electrolyte have many safety issues.[3] Replacement of the liquid electrolyte with a solid electrolyte and the assembly of all-solid-state lithium sulfur batteries is a good solution to eliminate the safety issues.[3] The three main components of the system include the cathode mixture, highly conduct solid electrolyte and compatible anode, which are essential in order to fabricate an all-solid-state Li–S battery which can be cycled effectively. Due to the non-liquid nature of the solid electrolyte, a large amount of the solid electrolyte needs to be introduced in the cathode mixture to enhance the ionic conductivity and enable an ionically conductive framework.[21] However, the roles of the solid electrolyte in the cathode mixture of all-solid-state Li–S batteries are not fully understood. It can not only promote the lithium ion conductivity of the cathode mixture, but also has the capability to act as a cathode material due to its lithium-containing components. Whether or not it can participate in the electrochemical reactions in the cathode mixture and its structural evolution process during cycling remains unknown.

In this work, detailed synthesis processes were investigated and the optimum annealing temperature for Li_6PS_5Br fabricated by the simple solid-state reaction is obtained. A detailed correlation between the annealing temperatures, phase compositions, structure, and the ionic conductivity of Li_6PS_5Br from the solid-state reaction route is investigated based on XRD, neutron diffraction, and AC impedance. All-solid-state Li–S batteries using S–C–Li_6PS_5Br as cathode mixture and the optimized Li_6PS_5Br as solid electrolyte combined with Li–In are assembled and cycled at different charge/discharge loop modes to unravel the role of Li_6PS_5Br in the cathode mixture. Special all-solid-state batteries using Li_6PS_5Br as both cathode and solid electrolyte in a combination with In are designed. *Ex situ* XRD and electrochemical characterization are performed to clarify our explanations.

Experimental

Reagent-grade Li_2S (99.98%, Sigma-Aldrich), P_2S_5 (99%, Sigma-Aldrich), and LiBr (99.0%, Sigma-Aldrich) crystalline powders were used as starting materials. The required amount of each starting material was sealed in a tungsten carbide (WC)-coated stainless-steel jar with 10 WC balls (8 g per ball) in an argon filled glovebox (H_2O, O_2 < 0.3 ppm) to minimize the reactivity of the sample with oxygen and moisture. The total weight of the starting mixture was approximately 3.0 g. The mixture was first ball milled with a speed of 110 rpm for 1 h to ensure the homogeneity of the obtained raw mixture, after which it was sealed in a quartz tube and annealed at various temperatures (250, 300, 350, 400, 500, 550, and 600 °C) for 10 hours to obtain

different annealed samples. The solid electrolytes (Li_6PS_5Br) used for the all-solid-state batteries in this work were annealed at 550 °C for 10 h. To prepare the LiBr excess Li_6PS_5Br, 10% and 15% weight excess of LiBr based on the required amount of LiBr was mixed with the stoichiometric Li_2S and P_2S_5 with rotation speed of 110 rpm for 1 h to obtain a homogenous mixture. Then the mixture was sealed in a quartz tube and annealed at 550 °C for 10 h. These two samples are named 10% excess-Li_6PS_5Br and 15% excess-Li_6PS_5Br, respectively.

Powder XRD patterns were collected over a 2θ range of 10–100° to identify the crystalline phases of the different samples using $Cu_{K\alpha}$ X-rays (1.5406 Å at 45 kV and 40 mA) on an X'Pert Pro X-ray diffractometer (PANalytical). To prevent reaction with moisture and oxygen, the powders were sealed in an airtight XRD sample holder in an argon filled glove box. Neutron diffraction data was collected on the new neutron powder diffractometer PEARL of the TU Delft. Data was collected at room temperature using the (533) reflection of the germanium monochromator (lambda = 1.665 Å). The sample was loaded under argon in a 6 mm diameter air-tight vanadium sample can. The sample was measured for 18 hours from 10.4–160 degrees 2θ. The data treatment consisted of a detection efficiency correction for each of the 1408 detector pixels and a subtraction of the background, caused by the instrument and the sample can. The neutron and X-ray data were refined simultaneously using the Rietveld method implemented in GSAS.[22,23] To investigate the structure evaluation of cathode mixture and the solid electrolyte layer, the assembled solid-state battery was first cycled to different stages and then dissembled. The cathode mixture and the solid electrolyte layer of this solid-state battery were collected and characterized by XRD using a Kapton-sealed sample holder.

The ionic conductivity of the mixture annealed at various temperatures was determined by AC impedance. Stainless-steel disks were attached on both faces of the 10 mm diameter powder pellet. AC impedance measurements were performed using an Autolab (PGSTAT302N) in the frequency range of 1 Hz to 1 MHz with an applied voltage of 0.01 V.

Laboratory-scale solid-state S–C–Li_6PS_5Br/Li_6PS_5Br/Li–In and Li_6PS_5Br–C/Li_6PS_5Br/In batteries were prepared. For the S–C–Li_6PS_5Br/Li_6PS_5Br/Li–In batteries, the S–C composite mixture was prepared according to our previous work.[10] For the Li_6PS_5Br–C/Li_6PS_5Br/In batteries, the Li_6PS_5Br was ball milled with Super P (TIMCAL) and carbon nano-fiber (Sigma-Aldrich) with a weight ratio of 70 : 15 : 15 first with the rotation of 110 rpm for 1 h followed by a higher rotation speed of 500 rpm for 4 h to obtain the final cathode mixture used for the solid-state battery. A two-layer pellet with a diameter of 10 mm, consisting of 5.5–7.0 mg of the described cathode mixture and 135–145 mg of the Li_6PS_5Br solid electrolyte, was obtained by pressing the electrode and electrolyte powders with 6 tons of pressure. A piece of In foil or Li–In alloy (d = 9.525 mm) were subsequently attached to the other side. Finally, the full solid-state battery pellet was pressed with 2 tons of pressure for 30 s. The assembled cell was charged and discharged with various current densities (0.064, 0.13, and 0.32 mA cm^{-2}) within specified voltage windows (0–3.0 V and 0–5.0 V *vs.* In) in order to evaluate the electrochemical

This journal is © The Royal Society of Chemistry 2019

J. Mater. Chem. A, 2019, **7**, 10412–10421 | **10413**

performance. The cyclic voltammetry (CV) measurements of the solid-state batteries were performed within the voltage windows of 0–3.0 V and 0–5.0 V $vs.$ In with a sweep speed of 0.2 mV s^{-1}. The obtained capacity in this work was normalized according to the weight of the Li_6PS_5Br in the cathode. All the cycling measurements for solid-state batteries in this work are performed at room temperature.

Results and discussion

To obtain the pure Li_6PS_5Br solid electrolyte via the simple solid-state reaction route, the mixed precursor was annealed at various temperatures (250–600 °C) for 10 h. The XRD and powder neutron diffraction Rietveld refinement results of these annealed samples are shown in Fig. 1 and 2. As shown in Fig. 1,
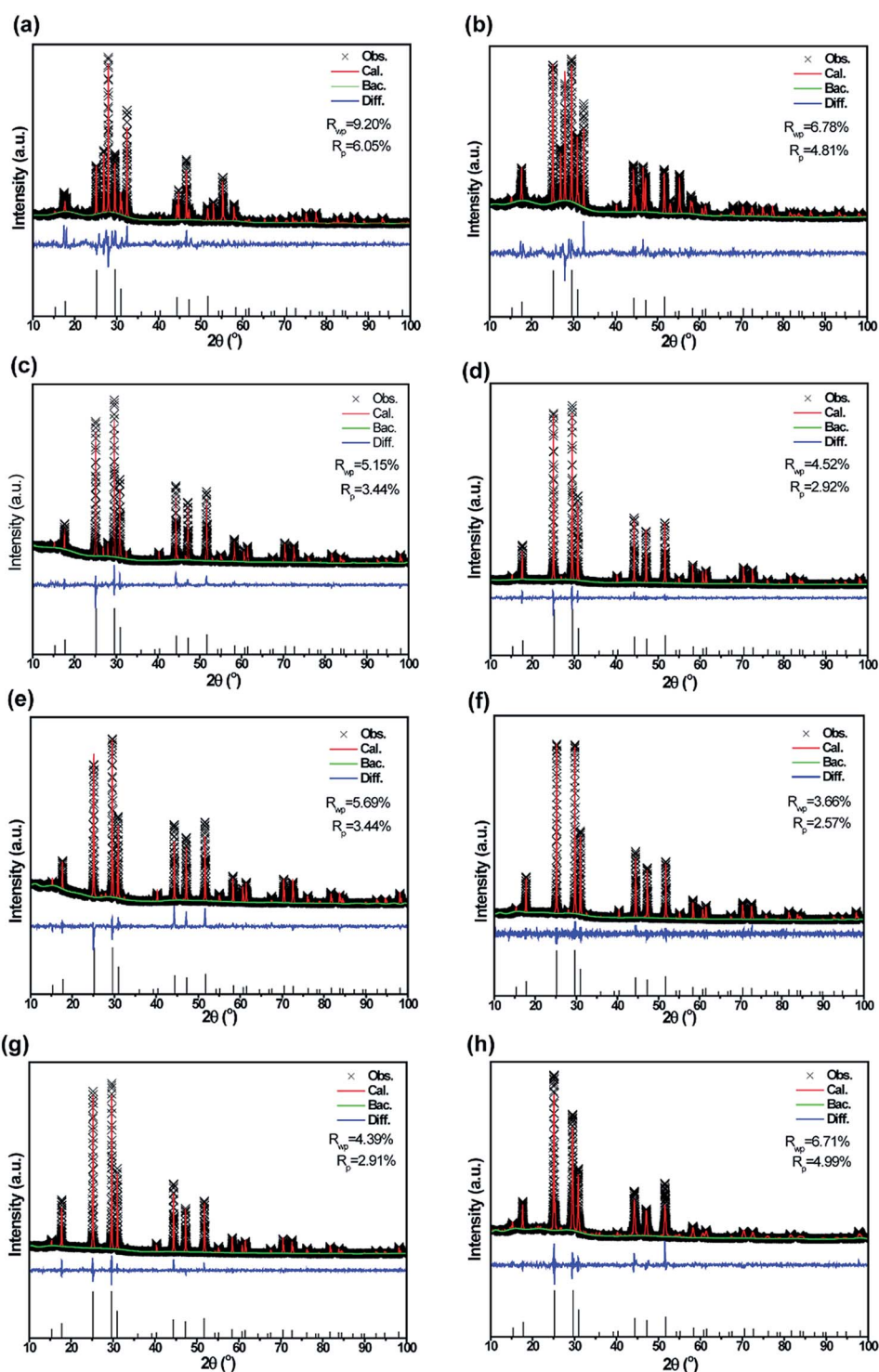

Fig. 1 Rietveld refinement results of XRD data for the products obtained by annealing of the raw mixture at various temperatures: (a) 250, (b) 300, (c) 350, (d) 400, (e) 450, (f) 500, (g) 550, and (h) 600 °C.
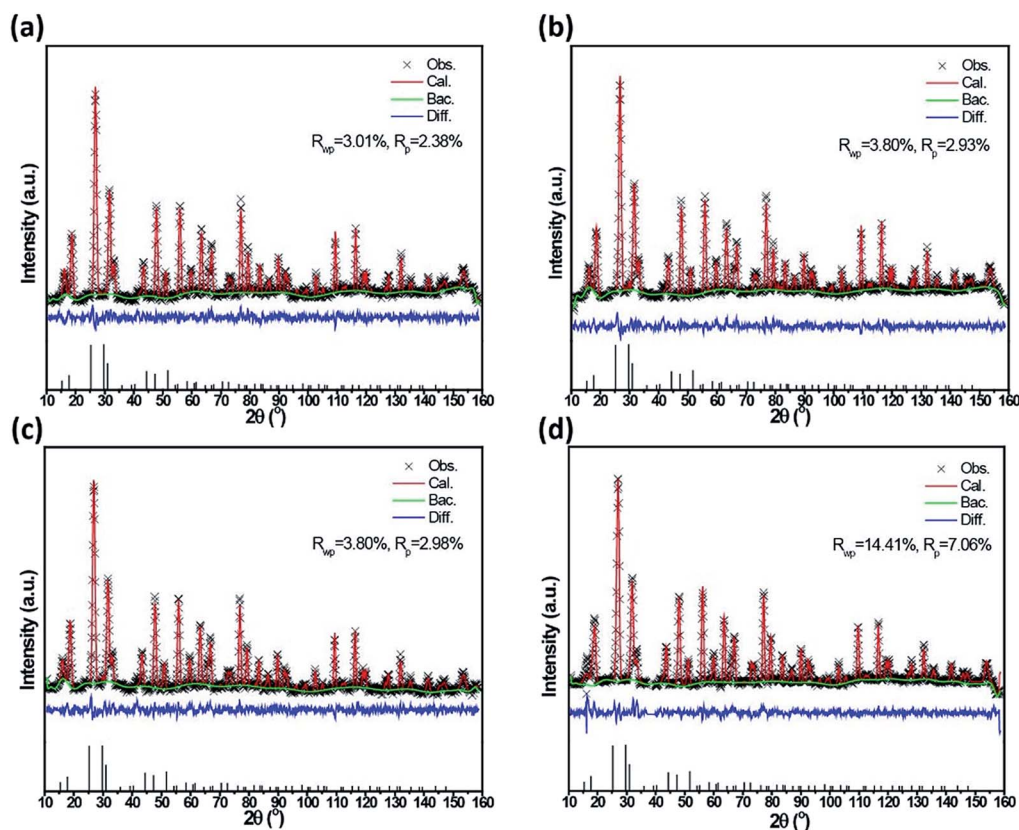
Fig. 2 Neutron diffraction patterns of the Li_6PS_5Br samples prepared by different annealing temperatures simultaneously refined by Rietveld refinement: (a) 400, (b) 450, (c) 500, and (d) 550 °C.

at lower temperatures (such as 250 and 300 °C), the diffractions are ascribed to the starting materials (Li_2S and $LiBr$). At higher annealing temperatures, the peak intensity due to Li_6PS_5Br reflections became strengthened, while the reflections from Li_2S and $LiBr$ decrease with increasing annealing temperatures.[8] When the annealing temperature is higher than 400 °C, the major diffraction peaks can be attributed to the target Li_6PS_5Br phase. For annealing temperatures at 500 and 550 °C, pure Li_6PS_5Br phase with a F43m structure is obtained,[8] which is clarified by both the XRD and Neutron diffraction, as shown in Fig. 1(f, g) and 2(c, d). When the annealing temperature reaches 600 °C, diffraction peaks due to the Li_2S and P_2S_5 phases were detected, which may be associated with the decomposition of the lithium argyrodite. Similar behavior is also found for Li_6PS_5Cl using the same solid-state reaction method.[7] The crystallographic parameters resulting from the refinements for samples annealed at the selected temperatures (400, 450, 500, 550, and 600 °C) are displayed in Table S1–S5.† It can be seen from these tables that the lattice constant (a) increased with increasing annealing temperature. Previous simulation results showed that there are three types of lithium jumps in lithium argyrodites; the doublet jump between paired 48 h sites, the inter-cage jump between different 48 h pairs, and the intra-cage jump between cages.[6,24] As a result, the distances for these three types of jumps provide vital information for the evaluation of lithium ion transport in Li_6PS_5X (X = Cl, Br). Such

kinds of jump distances can be obtained from the Rietveld refinement, as shown in Fig. 3. Kraft *et al.* demonstrated that the jump distances have a relationship with the lattice parameters.[5] The Li^+–Li^+ jump distances change as a function of the sintering temperatures were reported for Li_6PS_5Cl, showing similar evolution to the present results.[7] However, the lithium jump distances for Li_6PS_5Br are larger than that of Li_6PS_5Cl annealed at the same temperature and time duration, implying a lower lithium ion conductivity for the former,[7] which is in good agreement with the AC impedance results in the following section. Interestingly, for the sample annealed at 550 °C, the jump distances of three types in Li_6PS_5Br are quite similar, which may also be a sign of better lithium ion conductivity compared with other samples. Our previous work has reported that the inhomogeneous distribution of Br over the two crystallographic sites (4a and 4c) may be partially responsible for the larger Li-ion mobility at the interfaces.[8] Previous simulation results have reported that the highest Li-ion conductivity can be obtained when the occupation ratio of Cl over the 4a and 4c sites are close to 3.[24] In this work, as shown in Table S1–S5,† the occupation ratio of Br over the 4a and 4c sites for Li_6PS_5Br annealed at 400, 450, 500, 550, and 600 °C are 2.28, 2.89, 2.98, 3.01, and 2.35, respectively. Our experiment results showed that the Li-ion conductivity of Li_6PS_5Br depends on the Br ordering over 4a and 4c sites. The occupation ratio over 4a and 4c is closer to 3, the Li-ion conductivity is higher.
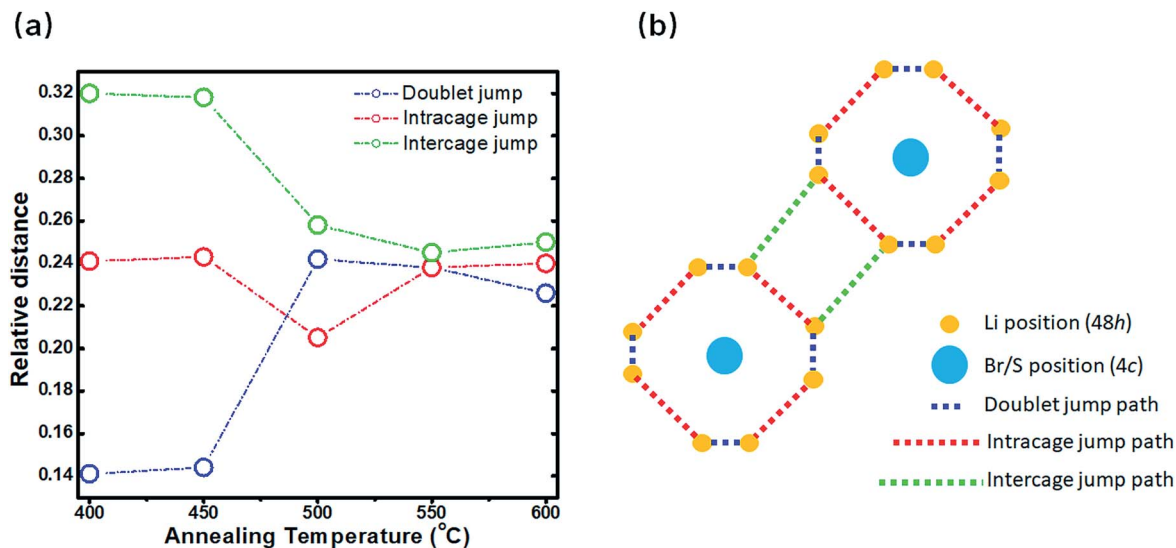
(a)

(b)

Fig. 3 (a) The Li^+–Li^+ jump distances in Li_6PS_5Br synthesized at various temperatures obtained from the Rietveld refinements of the neutron diffraction data. (b) 2D images of doublet jump, intracage jump, and intercage jump in Li_6PS_5Br.

To explore the correlation between annealing temperature and the lithium ion conductivity, AC impedance spectroscopy was applied in the temperature range between 25 and 120 °C. Fig. 4(a) shows the changes of lithium ion conductivity as a function of annealing temperatures. The room temperature ionic conductivities of the samples prepared by annealing at various temperatures are 8.06×10^{-5} S cm^{-1} for 250 °C, 2.28×10^{-4} S cm^{-1} for 300 °C, 7.98×10^{-4} S cm^{-1} for 350 °C, 1.15×10^{-3} S cm^{-1} for 400 °C, 1.38×10^{-3} S cm^{-1} for 450 °C, 1.65×10^{-3} S cm^{-1} for 500 °C, 2.58×10^{-3} S cm^{-1} for 550 °C, and 1.41×10^{-3} S cm^{-1} for 600 °C, respectively. As shown in the figure, the lithium ion conductivity increased with higher annealing temperatures, which is due to a decreasing of the starting materials (Li_2S and LiBr) and an increase of the target phase (Li_6PS_5Br) in the samples. The highest lithium ion conductivity was achieved by the sample annealed at 550 °C, which is in good agreement with previous structure analysis. For the sample annealed at 600 °C, a lower lithium ion conductivity was delivered compared to the sample annealed at 550 °C due to the decomposition of Li_6PS_5Br, which is confirmed by the XRD and Neutron diffraction results. Furthermore, the corresponding Arrhenius plots of the precursor after annealing at various temperatures are shown in Fig. 4(b), which shows results that are in good agreement with XRD and neutron diffraction analysis. When the annealing temperature reaches 350 °C, the target Li_6PS_5Br becomes the major phase in the sample, yielding much higher conductivities. Among the annealed samples, those treated at 550 °C show the highest lithium ion conductivity due to the high purity of the Li_6PS_5Br phase. The activation energies of the solid electrolyte samples obtained after annealing at various temperatures do not differ greatly, yields a value of 0.255 eV. Previous research has shown that the optimal sintering temperature for Li_6PS_5Cl using the simple solid-state method is also 550 °C, while the corresponding lithium ion conductivity of Li_6PS_5Cl is much higher than

Li_6PS_5Br in this work.[7] One possible explanation is that Li_6PS_5Br shows much larger lithium jump distances than that of Li_6PS_5Cl as we discussed in the former section. Rao et al. showed that in order to reach a room temperature conductivity of 1 mS cm^{-1} and low activation energy of 0.16 eV with the mechanical milling route, the milled samples had to be heat-treated with a temperature higher than 250 °C.[9] With this simple solid-state route to synthesize Li_6PS_5X (X = Cl, Br), it was found that it is necessary to anneal the precursors to higher than 400 °C to achieve lithium argyrodite with a lithium ionic conductivity close to 1 mS cm^{-1}.[7]

Unlike lithium sulfur battery using organic liquid electrolytes, solid-state Li–S battery required the introduction of solid electrolyte in the cathode mixture to provide ionic conductivity. Here, the prepared Li_6PS_5Br was chosen as the solid electrolyte to combine with S–C cathode material and a Li–In alloy anode to fabricate the all-solid-state Li–S batteries. A typical Li–S battery is required to start on discharge, corresponding to the extraction of lithium ions from the anode side, due to the fact that there are no lithium-containing materials in the cathode side. However, in the all-solid-state battery system, the situation is much more complicated because of the introduction of the lithium-containing solid electrolyte in the cathode mixture. Fig. 5(a) shows the first three (dis)charge curves of S–C–Li_6-PS_5Br/Li_6PS_5Br/Li–In all-solid-state battery. This battery was first cycled by discharging and followed by a subsequent charge at 0.13 mA cm^{-2} between 0 and 3 V vs. In. The initial discharge and charge capacities are 1523.60 and 737.11 mA h g^{-1}, respectively. The low initial coulombic efficiency (48.42%) suggests that more than half of the lithium ions extracted from the Li–In alloy anode cannot participate in the subsequent cycles. However, the second charge capacities are much higher than that of the initial capacity, implying part of the Li_6PS_5Br electrolyte in the cathode mixture may participate in the electrochemical reaction and provide capacity. One possible
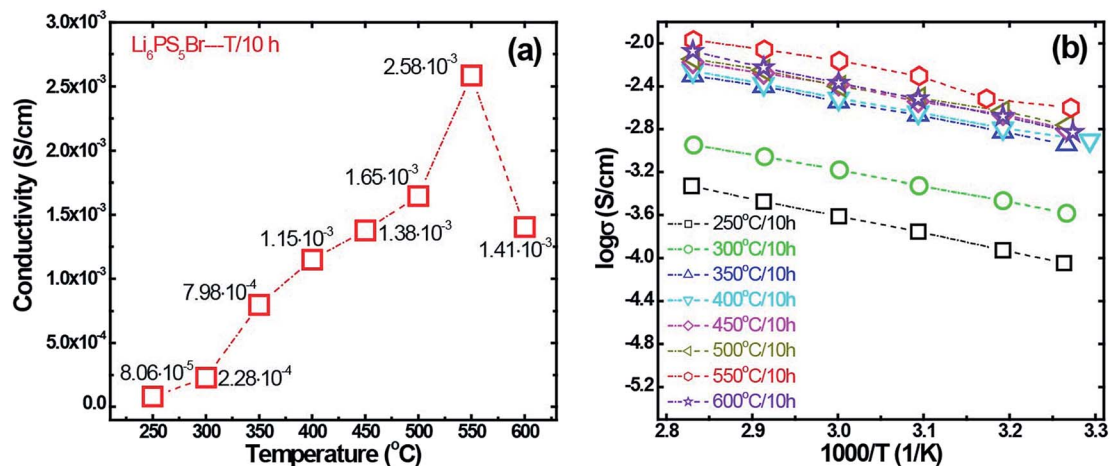
10416 | J. Mater. Chem. A, 2019, 7, 10412–10421

This journal is © The Royal Society of Chemistry 2019

Fig. 4 (a) Room temperature lithium ion conductivity of Li_6PS_5Br annealed at different temperatures. (b) The corresponding Arrhenius plots of Li_6PS_5Br annealed at different temperatures. The impedance spectrum was measured from room temperature to 100 °C.

explanation is that the capacity comes from the side-product Li_2S in the initial cycle, which can be reversible (dis)charged in the subsequent cycles. Another possible reason is that Li_6-PS_5Br in the cathode mixture may be involved to the activation processes of S–C cathode composite, and provide mobile lithium ions for the S–C cathode mixture. Moreover, the coulombic efficiencies of the second and the third cycle are much higher than that of the initial cycle, suggesting that the Li_6PS_5Br–C cathode mixture can reversible cycle in this all-solid-state battery, and the capacity of which may be associated with the side-product of the decomposition, such as Li_2S. The discharge plateau observed in Fig. 5 for all-solid-state Li–S batteries, located at ∼2.12 V *vs.* Li/Li^+,[25] is quite similar as that of Li_2S cathode in organic liquid electrolyte-based lithium ion batteries, suggesting that Li_2S is involved in the electrochemical reaction of all-solid-state Li–S batteries. When the upper cut-off

(dis)charge voltage is increased up to 5 V *vs.* In, similar charge capacity behavior is observed in the initial cycles. To verify our explanation, S–C–Li_6PS_5Br/Li_6PS_5Br/Li–In all-solid-state battery was first charged to 5 V *vs.* In and then discharge to 0 V *vs.* In, as displayed in Fig. 5(b). The initial charge capacity is 163.93 mA h g^{-1}, which is attributed to the decomposition of Li_6PS_5Br electrolyte in the cathode mixture and its side products. The initial discharge capacity is much higher than the charge capacity (882.87 mA h g^{-1} *vs.* 163.93 mA h g^{-1}), which suggests that lithium ions can still be extracted from the Li–In anode in this situation. However, the (dis)charge capacities achieved from this charge–discharge loop mode are much smaller than that of the discharge–charge loop mode, implying that solid electrolyte in the cathode mixture of all-solid-state Li–S battery is highly influenced by the charge/discharge loop mode.
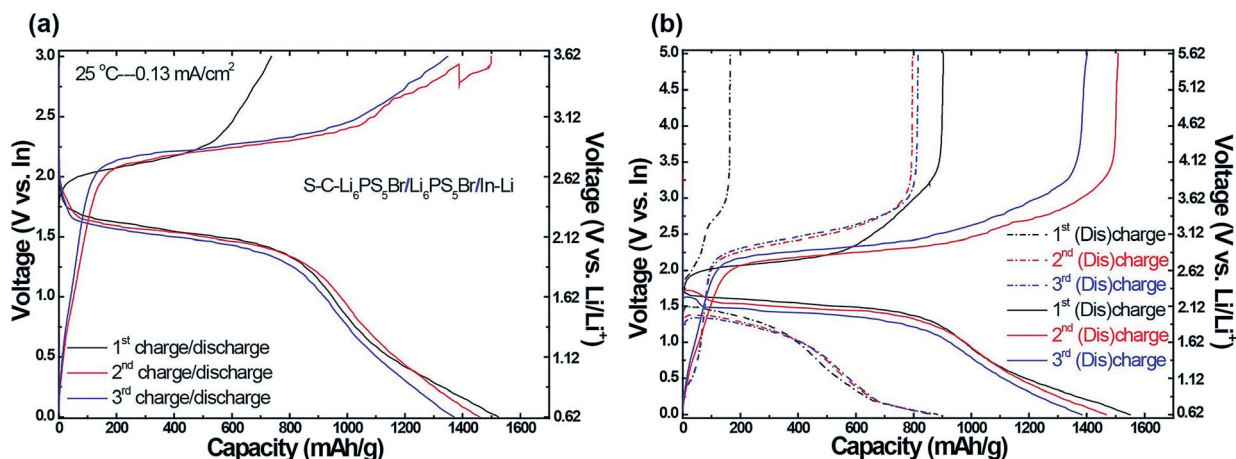

Fig. 5 (a) The charge/discharge curves of the first three cycles of S–C–Li_6PS_5Br/Li_6PS_5Br/In–Li solid-state batteries starting on discharge cycled at 0.13 mA cm^{-2} between 0 and 3.0 V *vs.* In. (b) The charge/discharge curves of the first three cycles of S–C–Li_6PS_5Br/Li_6PS_5Br/In–Li solid-state batteries cycled at 0.13 mA cm^{-2} between 0 and 5.0 V *vs.* In. For the solid lines, the solid-state Li–S battery was first discharged and then charged, while for the dashed line, the solid-state Li–S battery was first charged and then discharged. The capacities showed in the figure are calculated based on the weight of S in the cathode mixture.

To reveal the role of Li_6PS_5Br in the cathode mixture of the all-solid-state Li–S battery, the effect of charge/discharge loop mode needs to be eliminated. Therefore, a special solid-state battery design is required. Hereby, Li_6PS_5Br was chosen to work as both active material and solid electrolyte to assemble a Li_6PS_5Br–C/Li_6PS_5Br/In solid-state battery. The reason that In was chosen as the anode material was to ensure that Li_6PS_5Br is the only lithium source in the electrode mixtures during cycling. As shown in Fig. 6, the assembled battery was charged/discharged under 0.32 mA cm^{-2} within different voltage windows of 0–3 V and 0–5 V *vs.* In. When the battery was cycled between 0 and 3 V *vs.* In, as shown in Fig. 6(a), the initial charge and discharge capacities are 340.93 and 290.34 mA h g^{-1}, respectively. The initial coulombic efficiency is 85.16%, suggesting that only part of Li ions can participate in the electrochemical reaction and provide discharge capacity. This battery can deliver reversible capacity in the subsequent cycles with stable coulombic efficiencies. After 12 cycles, the corresponding charge and discharge capacities are 138.67 and 134.81 mA h g^{-1}. To unravel the electrochemical mechanism of this Li_6PS_5Br–C/Li_6PS_5Br/In solid-state battery, *ex situ* XRD was performed on the cathode mixture of this battery before and after various cycles to observe the structural evolutions. To ensure that all the reflection peaks come from

the cathode mixture, only whole pellets with homogenously distributed cathode layers were chosen to perform the XRD measurements. As shown in Fig. S3,† the major diffraction peaks belonging to Li_6PS_5Br are observed not only in the patterns after the initial charge and discharge cycles, but also in the pattern after 18 full cycles, suggesting that the Li_6PS_5Br phase is still present in the cathode mixture after cycling. Moreover, diffraction peaks indexed to Li_2S and LiBr are observed in the pattern, implying the decomposition of Li_6PS_5Br. After 18 cycles, the diffraction peaks belong to LiBr are still observed in the XRD pattern of the cycled cathode mixture. Since the capacity of this kind of battery was calculated based on the weight of Li_6PS_5Br in the cathode mixture, while the truly contribution of capacity from Li_6PS_5Br is decreased with cycling number due to the decomposition of Li_6PS_5Br, yielding lower discharge capacities for the subsequent cycles. The cyclability of Li_2S yielded from the decomposition of Li_6PS_5Br in the cathode mixture is unclear, which may have an influence in the coulombic efficiency behavior of both the Li_6PS_5Br–C/Li_6PS_5Br/In solid-state batteries in Fig. 6 and the S–C–Li_6PS_5Br/Li_6PS_5Br/Li–In all-solid-state batteries in Fig. 5. Another possible factor may also affect the coulombic efficiency is the In anode, which can act as a host material to accept the mobile Li ions from the cathode
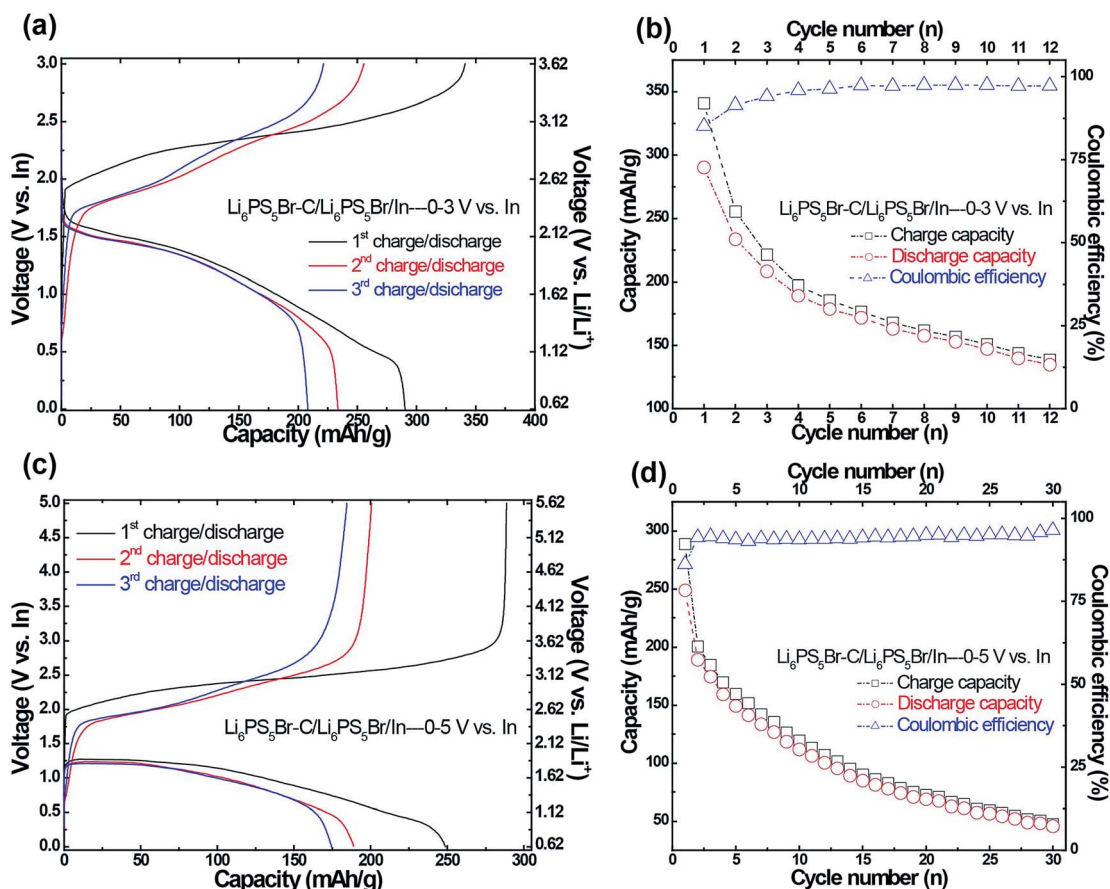

Fig. 6 Charge/discharge curves and cycling performances of Li_6PS_5Br–C/Li_6PS_5Br/In all-solid-state batteries at different voltage windows: (a and b) 0 and 3.0 V *vs.* In, (c and d) 0 and 5.0 V *vs.* In at the current density of 0.32 mA cm^{-2}.

10418 | *J. Mater. Chem. A*, 2019, **7**, 10412–10421

This journal is © The Royal Society of Chemistry 2019

mixture. Since the Li_6PS_5Br electrolyte in the cathode mixture is decomposed,[26–29] the question is raised as to how Li_6PS_5Br functions as the solid electrolyte. To verify this, *ex situ* XRD of Li_6PS_5Br using as the solid electrolyte in a Li_6PS_5Br–C/Li_6-PS_5Br/In solid-state Li–S battery was conducted before and after 3 cycles, as shown in Fig. S4.† After 3 cycles, the major diffraction peaks indexed to Li_6PS_5Br phase are observed, suggesting that the Li_6PS_5Br is stable during cycling when working as solid electrolyte in the all-solid-state Li–S battery. When a wider voltage window (0–5 V *vs.* In) was applied, lower charge and discharge capacities were obtained, 288.59 and 248.74 mA h g^{-1}, as shown in Fig. 6(c). The reason behind the lower capacities is likely due to decomposition of the Li_6PS_5Br in the cathode mixture, which yields LiBr and other amorphous phases that encapsulate Li_6PS_5Br particles and impeded the decomposition. Due to this blocking effect, Li_6-PS_5Br–C/Li_6PS_5Br/In solid-state battery show poor cycling performance, as shown in Fig. 6(d). Our assumption has also been proved by the EIS results displayed in Fig. S5.† When the upper cut-off charge/discharge voltage is increased to 5 V, resistances belong to the interfacial portion of the cathode mixture are quite obvious after 12 cycles, while for the battery cycled at lower cut-off voltage (3 V *vs.* In), the resistance caused by the interface part is not so clear, as shown in Fig. S5.† Additionally, cyclic voltammetry (CV) was also performed by scanning the Li_6PS_5Br–C/Li_6PS_5Br/In solid-state battery with a sweep rate of 0.2 mV s^{-1} at different voltage windows. As shown in Fig. S6,† the initial anodic peak locates at 2.5 V *vs.* In, corresponding to 3.1 V *vs.* Li/Li$^+$, can be attributed to the decomposition of Li_6PS_5Br in the cathode mixture. Another shoulder anodic peak in the initial cycle is observed in the initial cycle and disappeared in the subsequent anodic processes, which is unclear for us right now. The initial cathodic peak locates at 0.45–0.5 V *vs.* In, corresponding to 1.05–1.15 V *vs.* Li/Li$^+$, represents the reduction of S to higher order poly-sulphides as reported.[10] The amount of S in the cycled cathode mixture is really small, which makes it difficult to detect the diffraction peaks. Previous XPS results have reported that Li_6PS_5Cl is partially decomposed into LiCl, "P_2S_5", and Li_2S_n with an undetermined polysulfide average chain length n.[27] The cathodic peaks locate at 0.8–1.2 V *vs.* In may be associated with the reduction of Li_2S_n formed in the initial charging process. In the subsequent cycles, the anodic peaks locate at ∼2.0 V *vs.* In, which represents the oxidation of Li_2S to lower order poly-sulfides, shows highly reversible performances in the voltage window between 0 and 3 V *vs.* In. Other anodic peaks due to the decomposition of Li_6PS_5Br in the cathode mixture, located at ∼2.5 V *vs.* In, decrease with cycle number. This implies that the decomposition of Li_6PS_5Br happens continuously in the cathode mixture, not only during the initial charge process, and becomes weaker in subsequent cycles. However, when the upper cut-off voltage is increased to 5.0 V *vs.* In, the anodic peaks due to the decomposition of Li_6PS_5Br are only observed in the first few cycles (less than 5), suggesting that the decomposition of Li_6PS_5Br is impeded, which is in good agreement with previous battery performances. Moreover, due to the blocking of Li_6PS_5Br

decomposition, the anodic peaks belonging to the oxidation of Li_2S also weaken. Correspondingly, the discharge capacity of Li_6PS_5Br–C/Li_6PS_5Br/In solid-state battery decrease intensely with cycling numbers, as shown in Fig. 6(b).

Previous research has reported that battery performance of sulfide-based solid-state battery using Li_2S as active can be enhanced by introducing a small amount of LiX (X = Cl, Br).[30] In our battery system, Li_2S is present in the cathode mixture when Li_6PS_5Br–C/Li_6PS_5Br/In solid-state battery is cycled between 0 and 3 V *vs.* In due to the decomposition of Li_6PS_5Br. To verify the explanation mentioned in the former section, an excess of LiBr is introduced in the Li_6PS_5Br electrolyte from the synthesis section. The obtained materials were chosen as the cathode mixture to assemble all-solid-state Li–S batteries. As shown in Fig. S7,† the room temperature lithium ion conductivities of 10% excess-Li_6PS_5Br and 15% excess-Li_6PS_5Br are 9.01 × 10^{-4} and 1.06 × 10^{-3} S cm^{-1}, both of which are lower than the 2.58 × 10^{-3} S cm^{-1} obtained for Li_6PS_5Br synthesized by annealing the stoichiometric starting material. The corresponding activation energies of the 10% excess- and 15% excess-LiBr samples are 0.298 and 0.324 eV, both of which are higher than 0.255 eV for Li_6PS_5Br without excess LiBr. It is concluded that introducing excess LiBr in the raw material will not only decrease the lithium ion conductivity of Li_6PS_5Br, but also increase the energy barrier.

Fig. 7 shows the first three (dis)charge curves and the cycling performance of all-solid-state batteries using Li_6PS_5Br as the solid electrolytes in combination with In anode and various active materials. Li_6PS_5Br, 10% excess, and 15% excess Li_6PS_5Br are chosen as the active materials. All of the assembled batteries are cycled at 0.13 mA cm^{-2} between 0 and 3 V *vs.* In, corresponding to 0.62 and 3.62 V *vs.* Li/Li$^+$. As shown in Fig. 7, the initial charge and discharge capacities of the solid-state battery using Li_6PS_5Br–C as the cathode are 345.30 and 307.14 mA h g^{-1}, respectively. The initial coulombic efficiency is 88.95%. When using 10% excess-Li_6PS_5Br and 15% excess-Li_6PS_5Br as active materials, the initial charge and discharge capacities are 383.06 and 358.98 mA h g^{-1} for 10% excess, and 349.68 and 325.74 mA h g^{-1} for 15% excess, respectively. Furthermore, an initial coulombic efficiency of 93.71% and 93.15% can be delivered by cells with 10% excess-Li_6PS_5Br and 15% excess-Li_6PS_5Br, respectively. After 35 cycles, the discharge capacity of the battery using Li_6PS_5Br as an active material is 157.03 mA h g^{-1}, delivering a capacity retention of 51.12%. In comparison, the corresponding values for the 10% excess-Li_6PS_5Br battery are 204.06 mA h g^{-1} and 58.36%, while the 15% excess-Li_6PS_5Br battery yields values of 170.08 mA h g^{-1} and 52.21%. From these data comparisons, it can be concluded that the introduction of LiBr in the cathode mixture of the Li_6PS_5Br–C/Li_6PS_5Br/In solid-state batteries can not only promote greater (dis)charge capacities but also can improve the cyclability. This results once again proves that it is Li_2S that functions as the active material in the cathode side of the Li_6PS_5Br–C/Li_6PS_5Br/In solid-state batteries, which is in good agreement with our former discussions.

This journal is © The Royal Society of Chemistry 2019

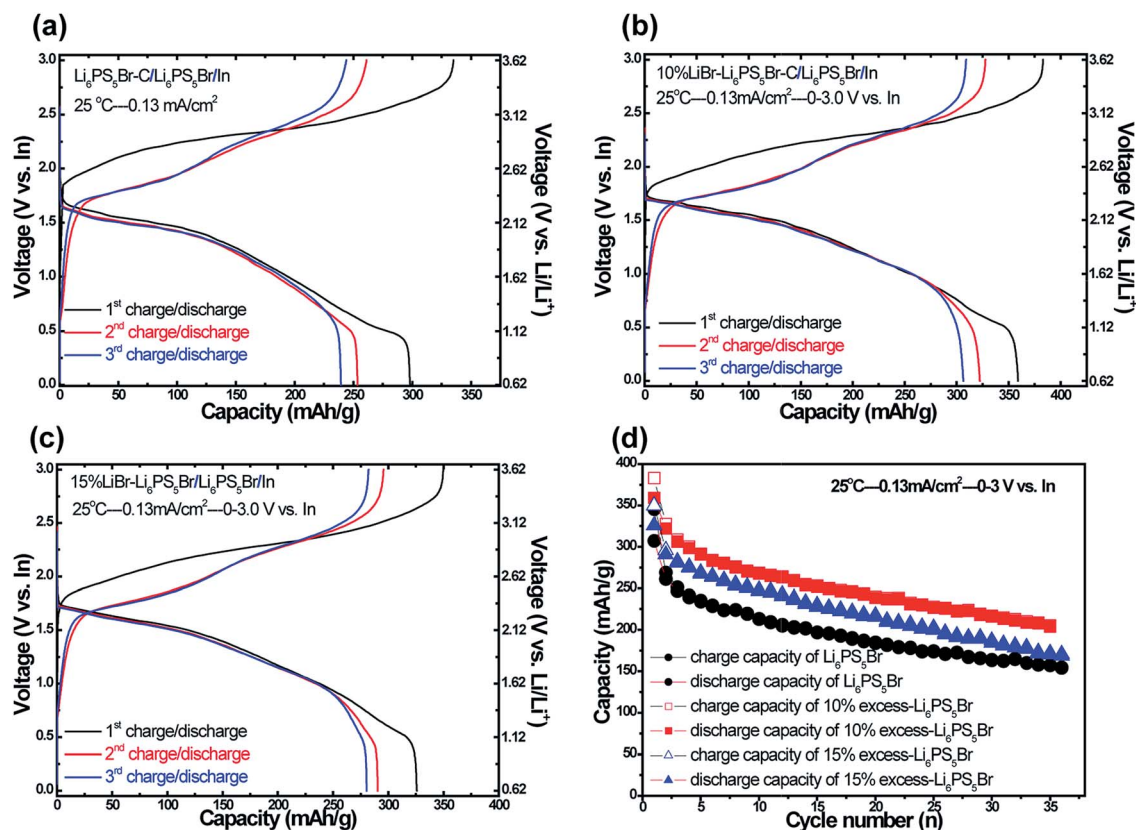*J. Mater. Chem. A*, 2019, **7**, 10412–10421 | **10419**

Fig. 7 Charge/discharge curves and cycling performances of Li$_6$PS$_5$Br−C/Li$_6$PS$_5$Br/In solid-state batteries using different cathode mixtures: (a) Li$_6$PS$_5$Br, (b) 10% excess-Li$_6$PS$_5$Br, (c) 15% excess-Li$_6$PS$_5$Br. (d) The corresponding cycling performances. These batteries were cycled at 0.13 mA cm^{-2} between 0 and 3 V vs. In.

Conclusions

Li$_6$PS$_5$Br with an ionic conductivity of 2.58×10^{-3} S cm^{-1} at room temperature was obtained by annealing the precursors acquired from simple direct milling of the raw materials at a low rotation speed. Structural and conductivity analysis showed that in order to achieve Li$_6$PS$_5$Br with an ionic conductivity close to 1 mS cm^{-1} using this simple solid-state reaction route, the heat treatment temperature should be higher than 400 °C. Neutron diffraction results suggest three kinds of jumps in Li$_6$PS$_5$Br; the doublet jump, the inter-cage jump, and the intra-cage jumps, which directly correlate to the ionic conductivity and are influenced by the annealing temperatures. A high Li-ion conductivity can be achieved when the Br ordering over 4a and 4c sites ratio is close to 3. The capacity of the Li$_6$PS$_5$Br-based all-solid-state Li–S batteries arises from two separate contributions, which include the active materials and the solid electrolyte in the cathode mixture.

Conflicts of interest

There are no conflicts to declare.

Acknowledgements

References

1 V. Etacheri, R. Marom, R. Elazari, G. Salitra and D. Aurbach, Challenges in the development of advanced Li-ion batteries: a review, *Energy Environ. Sci.*, 2011, **4**(9), 3243–3262.

2 E. P. Roth and C. J. Orendorff, How electrolytes influence battery safety, *Electrochem. Soc. Interface*, 2012, **21**(2), 45–49.

3 J. Yue, M. Yan, Y. X. Yin and Y. G. Guo, Progress of the Interface Design in All-Solid-State Li–S Batteries, *Adv. Funct. Mater.*, 2018, 1707533.

4 H. J. Deiseroth, S. T. Kong, H. Eckert, J. Vannahme, C. Reiner, T. Zaiß and M. Schlosser, Li$_6$PS$_5$X: A Class of Crystalline Li-Rich Solids With an Unusually High Li$^+$ Mobility, *Angew. Chem., Int. Ed.*, 2008, **47**(4), 755–758.

5 M. A. Kraft, S. P. Culver, M. Calderon, F. Böcher, T. Krauskopf, A. Senyshyn, C. Dietrich, A. Zevalkink, J. r. Janek and W. G. Zeier, Influence of Lattice Polarizability on the Ionic Conductivity in the Lithium

Superionic Argyrodites Li_6PS_5X (X= Cl, Br, I), *J. Am. Chem. Soc.*, 2017, **139**(31), 10909–10918.

6 C. Yu, S. Ganapathy, N. J. J. de Klerk, I. Roslon, E. R. H. van Eck, A. P. M. Kentgens and M. Wagemaker, Unravelling Li-Ion Transport from Picoseconds to Seconds: Bulk *versus* Interfaces in an Argyrodite Li_6PS_5Cl–Li_2S All-Solid-State Li-Ion Battery, *J. Am. Chem. Soc.*, 2016, **138**, 11192–11201.

7 C. Yu, S. Ganapathy, J. Hageman, L. van Eijck, E. R. van Eck, L. Zhang, T. Schwietert, S. Basak, E. M. Kelder and M. Wagemaker, Facile Synthesis toward the Optimal Structure-Conductivity Characteristics of the Argyrodite Li_6PS_5Cl Solid-State Electrolyte, *ACS Appl. Mater. Interfaces*, 2018, **10**(39), 33296–33306.

8 C. Yu, S. Ganapathy, E. R. H. van Eck, L. van Eijck, S. Basak, Y. Liu, L. Zhang, H. Zandbergen and M. Wagemaker, Revealing the relation between the structure, Li-ion conductivity and solid-state battery performance of the argyrodite Li_6PS_5Br solid electrolyte, *J. Mater. Chem. A*, 2017, **5**(40), 21178–21188.

9 R. P. Rao, N. Sharma, V. Peterson and S. Adams, Formation and conductivity studies of lithium argyrodite solid electrolytes using *in situ* neutron diffraction, *Solid State Ionics*, 2013, **230**, 72–76.

10 C. Yu, L. van Eijck, S. Ganapathy and M. Wagemaker, Synthesis, structure and electrochemical performance of the argyrodite Li_6PS_5Cl solid electrolyte for Li-ion solid state batteries, *Electrochim. Acta*, 2016, **215**, 93–99.

11 R. P. Rao and S. Adams, Studies of lithium argyrodite solid electrolytes for all-solid-state batteries, *Phys. Status Solidi A*, 2011, **208**(8), 1804–1807.

12 S. Boulineau, M. Courty, J.-M. Tarascon and V. Viallet, Mechanochemical synthesis of Li-argyrodite Li_6PS_5X (X= Cl, Br, I) as sulfur-based solid electrolytes for all solid state batteries application, *Solid State Ionics*, 2012, **221**, 1–5.

13 S. Boulineau, J.-M. Tarascon, J.-B. Leriche and V. Viallet, Electrochemical properties of all-solid-state lithium secondary batteries using Li-argyrodite Li_6PS_5Cl as solid electrolyte, *Solid State Ionics*, 2013, **242**, 45–48.

14 D. H. Kim, D. Y. Oh, K. H. Park, Y. E. Choi, Y. J. Nam, H. A. Lee, S.-M. Lee and Y. S. Jung, Infiltration of solution-processable solid electrolytes into conventional Li-ion-battery electrodes for all-solid-state Li-ion batteries, *Nano Lett.*, 2017, **17**(5), 3013–3020.

15 S. Yubuchi, M. Uematsu, M. Deguchi, A. Hayashi and M. Tatsumisago, Lithium-Ion-Conducting Argyrodite-Type Li_6PS_5X (X= Cl, Br, I) Solid Electrolytes Prepared by a Liquid-Phase Technique Using Ethanol as a Solvent, *ACS Appl. Energy Mater.*, 2018, **1**(8), 3622–3629.

16 L. Zhou, K.-H. Park, X. Sun, F. Lalere, T. Adermann, P. Hartmann and L. F. Nazar, Solvent-engineered Design of Argyrodite Li_6PS_5X (X= Cl, Br, I) Solid Electrolytes with High Ionic Conductivity, *ACS Energy Lett.*, 2019, **4**(1), 265–270.

17 S. Yubuchi, M. Uematsu, C. Hotehama, A. Sakuda, A. Hayashi and M. Tatsumisago, Argyrodite sulfide-based superionic conductor synthesized by liquid-phase technique with tetrahydrofuran and ethanol, *J. Mater. Chem. A*, 2019, **7**, 558–566.

18 S. Chida, A. Miura, N. C. Rosero-Navarro, M. Higuchi, N. H. Phuc, H. Muto, A. Matsuda and K. Tadanaga, Liquid-phase synthesis of Li_6PS_5Br using ultrasonication and application to cathode composite electrodes in all-solid-state batteries, *Ceram. Int.*, 2018, **44**(1), 742–746.

19 S. Yubuchi, S. Teragawa, K. Aso, K. Tadanaga, A. Hayashi and M. Tatsumisago, Preparation of high lithium-ion conducting Li_6PS_5Cl solid electrolyte from ethanol solution for all-solid-state lithium batteries, *J. Power Sources*, 2015, **293**, 941–945.

20 J. Wang, J. Yang, J. Xie and N. Xu, A novel conductive polymer–sulfur composite cathode material for rechargeable lithium batteries, *Adv. Mater.*, 2002, **14**(13–14), 963–965.

21 X. Yao, N. Huang, F. Han, Q. Zhang, H. Wan, J. P. Mwizerwa, C. Wang and X. Xu, High-Performance All-Solid-State Lithium–Sulfur Batteries Enabled by Amorphous Sulfur-Coated Reduced Graphene Oxide Cathodes, *Adv. Energy Mater.*, 2017, **7**(17), 1602923.

22 A. C. Larson and R. B. Von Dreele, *Gsas. General Structure Analysis System*, LANSCE, MS-H805, Los Alamos, New Mexico 1994.

23 B. H. Toby and R. B. Von Dreele, GSAS-II: the genesis of a modern open-source all purpose crystallography software package, *J. Appl. Crystallogr.*, 2013, **46**(2), 544–549.

24 N. J. de Klerk, I. Rosłoń and M. Wagemaker, Diffusion Mechanism of Li Argyrodite Solid Electrolytes for Li-Ion Batteries and Prediction of Optimized Halogen Doping: The Effect of Li Vacancies, Halogens, and Halogen Disorder, *Chem. Mater.*, 2016, **28**(21), 7955–7963.

25 S. Zhang, M. Liu, F. Ma, F. Ye, H. Li, X. Zhang, Y. Hou, Y. Qiu, W. Li and J. Wang, A high energy density Li 2 S@C nanocomposite cathode with a nitrogen-doped carbon nanotube top current collector, *J. Mater. Chem. A*, 2015, **3**(37), 18913–18919.

26 S. Wenzel, S. J. Sedlmaier, C. Dietrich, W. G. Zeier and J. Janek, Interfacial reactivity and interphase growth of argyrodite solid electrolytes at lithium metal electrodes, *Solid State Ionics*, 2018, **318**, 102–112.

27 J. Auvergniot, A. Cassel, D. Foix, V. Viallet, V. Seznec and R. Dedryvère, Redox activity of argyrodite Li_6PS_5Cl electrolyte in all-solid-state Li-ion battery: An XPS study, *Solid State Ionics*, 2017, **300**, 78–85.

28 J. Auvergniot, A. Cassel, J.-B. Ledeuil, V. Viallet, V. Seznec and R. Dedryvère, Interface Stability of Argyrodite Li_6PS_5Cl toward $LiCoO_2$, $LiNi_{1/3}Co_{1/3}Mn_{1/3}O_2$, and $LiMn_2O_4$ in Bulk All-Solid-State Batteries, *Chem. Mater.*, 2017, **29**(9), 3883–3890.

29 T. Cheng, B. V. Merinov, S. Morozov and W. A. Goddard III, Quantum Mechanics Reactive Dynamics Study of Solid Li-Electrode/Li_6PS_5Cl-Electrolyte Interface, *ACS Energy Lett.*, 2017, **2**(6), 1454–1459.

30 T. Hakari, A. Hayashi and M. Tatsumisago, Li_2S-Based Solid Solutions as Positive Electrodes with Full Utilization and Superlong Cycle Life in All-Solid-State Li/S Batteries, *Adv. Sustainable Syst.*, 2017, **1**(6), 1700017.

This journal is © The Royal Society of Chemistry 2019

J. Mater. Chem. A, 2019, **7**, 10412–10421 | **10421**